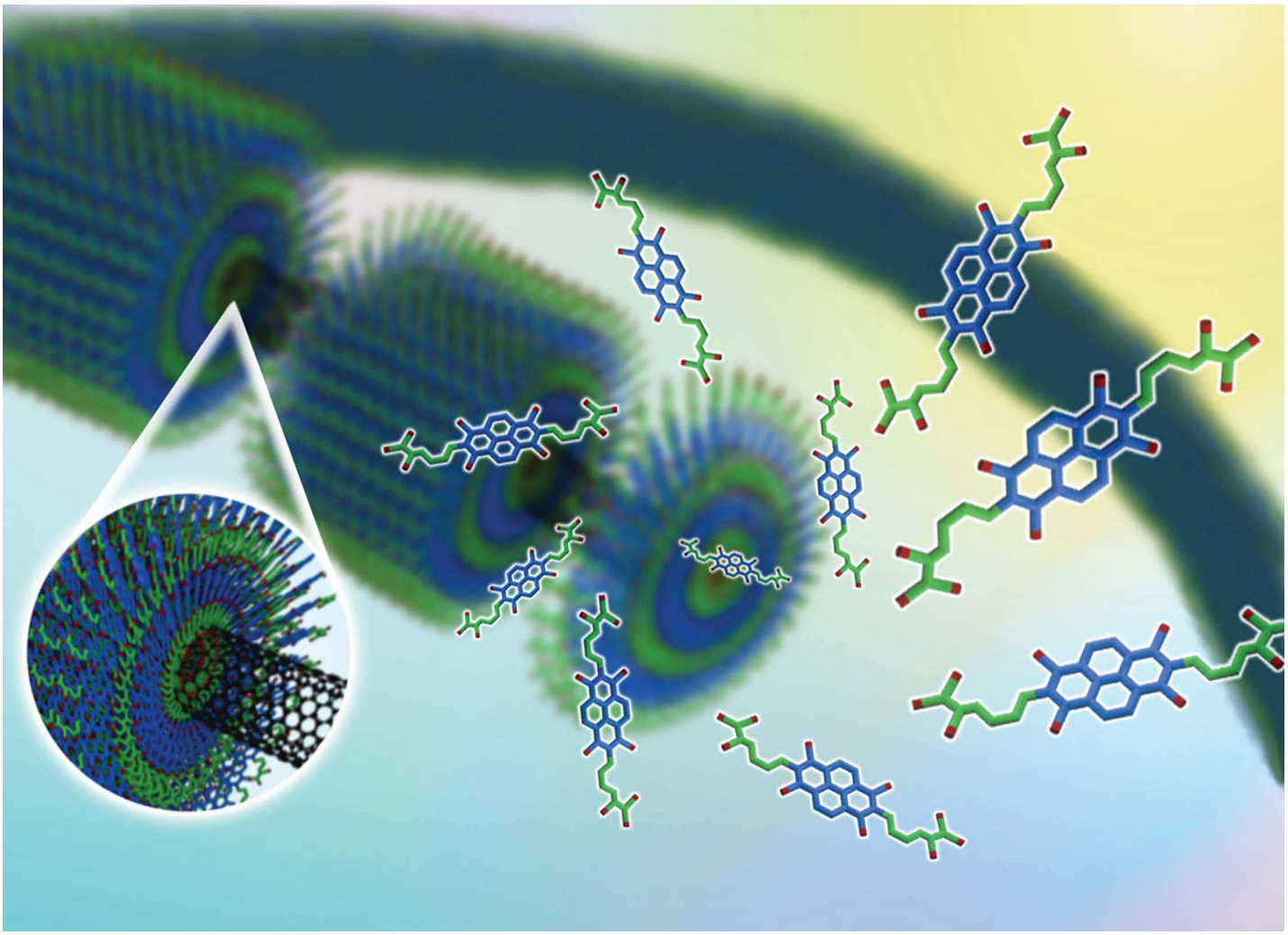

Showcasing research from Professor Parquette's laboratory, Department of Chemistry and Biochemistry, The Ohio State University, USA.

Threading carbon nanotubes through a self-assembled nanotube

Single-walled carbon nanotubes (SWNTs) are completely encapsulated by nanotubes formed by the self-assembly of naphthalenetetracarboxylic acid diimide (NDI)-lysine bolaamphiphiles. In this research, J. R. Parquette and co-workers show that self-assembled nanotubes, shortened by sonication-induced scission, efficiently coat SWNTs via electrostatic and cation-π interactions. Due to the ability of supramolecular materials to experience self-healing, the shortened nanotubes aligned along the SWNT surface grow and merge together, resulting in a homogeneous array of coaxial composites of carbon nanotubes threaded through self-assembled nanotubes.

As featured in:

See Jon R. Parquette *et al.*, *Chem. Sci.*, 2019, **10**, 7868.

ROYAL SOCIETY OF CHEMISTRY | Celebrating IYPT 2019

rsc.li/chemical-science

Registered charity number: 207890

Chemical Science

EDGE ARTICLE

View Article Online
View Journal | View Issue

Check for updates

Cite this: *Chem. Sci.*, 2019, **10**, 7868

All publication charges for this article have been paid for by the Royal Society of Chemistry

Threading carbon nanotubes through a self-assembled nanotube†

Mingyang Ji, [a] McKensie L. Mason, [a] David A. Modarelli [b] and Jon R. Parquette *[a]

Received 10th May 2019
Accepted 31st July 2019

DOI: 10.1039/c9sc02313e

rsc.li/chemical-science

Achieving the co-assembly of more than one component represents an important challenge in the drive to create functional self-assembled nanomaterials. Multicomponent nanomaterials comprised of several discrete, spatially sorted domains of components with high degrees of internal order are particularly important for applications such as optoelectronics. In this work, single-walled carbon nanotubes (SWNTs) were threaded through the inner channel of nanotubes formed by the bolaamphiphilic self-assembly of a naphthalenediimide-lysine (NDI-Bola) monomer. The self-assembly process was driven by electrostatic interactions, as indicated by ζ-potential measurements, and cation–π interactions between the surface of the SWNT and the positively charged, NDI-Bola nanotube interior. To increase the threading efficiency, the NDI-Bola nanotubes were fragmented into shortened segments with lengths of <100 nm *via* sonication-induced shear, prior to co-assembly with the SWNTs. The threading process created an initial composite nanostructure in which the SWNTs were threaded by multiple, shortened segments of the NDI-Bola nanotube that progressively re-elongated along the SWNT surface into a continuous radial coating around the SWNT. The resultant composite structure displayed NDI-Bola wall thicknesses twice that of the parent nanotube, reflecting a bilayer wall structure, as compared to the monolayer structure of the parent NDI-Bola nanotube. As a final, co-axial outer layer, poly(*p*-phenyleneethynylene) (PPE-SO_3Na, $M_W = 5.76 \times 10^4$, PDI – 1.11) was wrapped around the SWNT/NDI-Bola composite resulting in a three-component (SWNT/NDI-Bola/PPE-SO_3Na) composite nanostructure.

Open Access Article. Published on 01 August 2019. Downloaded on 10/13/2019 1:23:07 AM.
This article is licensed under a Creative Commons Attribution-NonCommercial 3.0 Unported Licence.

Introduction

The functional competence of synthetic materials that mimic nature depends on the precise positioning and synergistic action of multiple, discrete components, which are organized within higher order structures.[1–4] Composite nanomaterials have shown remarkable potential for applications in biomedicine,[5,6] catalysis[7–11] and energy conversion.[12–14] The physical properties of these systems critically rely on the topological and spatial relationships of each domain within the composite.[15,16] However, assembling multicomponent nanomaterials with this level of positional dexterity is hampered by the complexity of self-assembly.[17–19] There is a critical need for new strategies to assemble composite structures comprised of multiple classes of nanomaterials with nanoscale precision.[20–26] In this work, we describe the co-assembly of carbon nanotubes (CNTs), self-assembled nanotubes and polymers into a single, co-axial nanotube.

Highly efficient optoelectronic materials contain segregated, bicontinuous arrays of donor and acceptor nanodomains, but are challenging to create by self-assembly.[27–37] Single-walled carbon nanotubes (SWNTs) have continuous 1D structures that exhibit electronic properties ideally suited for optoelectronic applications.[38] However, the detrimental bundling and insolubility of SWNTs severely restricts the processability and performance of devices containing SWNTs. Polymer-wrapping has proven to be a versatile strategy to reduce bundling and enhance the solubility of SWNTs, as well to impart favorable electronic and mechanical properties.[39–42] However, the carbon nanotube–polymer interface is often weak and the long-range structure of the polymer segment is hard to control.[43] For example, a prior study demonstrated that one polymer could displace another on a SWNT surface.[44] The competitive binding between SWNTs and different polymers, along with the potential for the interpenetration of polymer layers, complicate the implementation of this strategy to construct ordered nanostructures comprised of multiple, self-sorted components.[44–46]

Peptides have also been developed to encapsulate SWNTs as a method to modify their surfaces. For example, peptide amphiphiles were assembled onto the surface of carbon

[a]*Department of Chemistry, The Ohio State University, 100 W. 18th Ave., Columbus, Ohio 43210, USA. E-mail: parquette.1@osu.edu*

[b]*Department of Chemistry, Center for Laser and Optical Spectroscopy, Knight Chemical Laboratory, The University of Akron, Akron, Ohio 44325-3601, USA*

† Electronic supplementary information (ESI) available: Assembly of composite nanostructures by TEM, AFM, UV, CD emission, Raman, and ζ-potential measurements; and force separation curves of DMT modulus studies. See DOI: 10.1039/c9sc02313e

This journal is © The Royal Society of Chemistry 2019

Open Access Article. Published on 01 August 2019. Downloaded on 10/13/2019 1:23:07 AM.
This article is licensed under a Creative Commons Attribution-NonCommercial 3.0 Unported Licence.

nanotubes in a manner that projected the hydrophilic peptide sequence toward the aqueous interface, thereby dispersing the nanotubes in water.[47] Similarly, alpha-helical, coiled-coil peptide barrels have been shown to encapsulate carbon nanotubes within their internal pores.[48] Single molecules were wrapped around the SWNTs by incorporating recognition units within U-shaped acyclic precursors to provide a strong binding interaction, then using metathesis reactions to close the rings and introduce a robust, mechanical link between the two components.[49,50] Similarly, Dieckmann developed a class of amphiphilic peptides that closed around the circumference of the SWNTs by reversible disulfide bond formation.[51] A recent computational study suggested that interpeptide β-sheet interactions stabilized the stacks of cyclized peptides.[52] The formation of interlocked CNT complexes by a "ring toss" method that threaded preformed cyclic compounds over CNTs has also been achieved.[53] These examples illustrate how CNTs can be wrapped by small molecular rings formed by covalent cyclization. A recent approach cyclized self-assembled, macrocyclic rings around CNTs *via* intermolecular hydrogen-bond formation.[54]

The self-assembly of surfactants into supramolecular structures on the surface of carbon nanotubes represents an early method to create stable CNT suspensions in water *via* non-covalent interactions.[55] Self-assembly offers several advantages as a strategy to encapsulate SWNTs. The highly reversible nature of the self-assembly process allows for dynamic error correction and energy minimization, resulting in a thermodynamically optimized composite structure with high water solubility and more complete coverage. The high degree of π–π stacking in the self-assembled coating thus leads to a hierarchically ordered structure with π-conjugation in both domains of the composite. Our approach relies on the self-assembly of NDI-Bola, which forms highly uniform nanotubes in water projecting polar zwitterionic head groups on the surface and in the internal pore of the nanotube.[56] In this work, we show that the self-assembly of NDI-Bola nanotubes efficiently encapsulates SWNTs *via* electrostatic and cation–π interactions, resulting in a homogeneous array of coaxial composites of carbon nanotubes threaded through self-assembled nanotubes. A ternary coaxial composite was then created by introducing an outer semiconducting polymer layer.

Results and discussion

Previously, we reported the self-assembly of NDI-Bola into well-defined nanotubes in water.[56] Self-assembly proceeded *via* the initial formation of monolayer rings that progressively stacked into well-defined nanotubes with inner diameters of ~7 nm and wall thicknesses of 2.5 ± 0.5 nm. The interior of the NDI-Bola nanotubes is highly polar due to the amino acid headgroups of the monomer and might be expected to be incompatible with the hydrophobic surface of a carbon nanotube. However, the π-electron-rich surface of SWNTs has recently been shown to bind to cations such as sodium[57,58] and mediate their migration,[59] presumably *via* a cation–π interaction.[60,61] Thus, the potential for cation–π interactions between protonated headgroups of the NDI-Bola interior and the SWNT surface prompted us to explore the ability of NDI-Bola to encapsulate the carbon nanotubes. Accordingly, NDI-Bola nanotubes were mixed with pristine, commercial SWNTs (60–70%; bundles, 2–10 nm; individual SWNT diameters, 1.55 nm (RBM), 2.1–2.3 (TEM) see Fig. S1†) and repeatedly sonicated until the mixture formed a homogeneous dispersion. Imaging the dispersion by transmission electron microscopy (TEM) revealed individual SWNTs encapsulated by the NDI-Bola nanotube fragments and protruding from the ends (Fig. S2†). The ζ-potential of the resulting pristine SWNT/NDI-Bola dispersion (pH 3.22) was 40.4 ± 4.0 mV, similar to that of the precursor NDI-Bola nanotubes (ζ = 45.5 ± 6.6 mV) under similar conditions (1 mM, pH 3.16) (Fig. S3†). The insignificant change in ζ-potential upon encapsulation of pristine SWNTs suggested that binding was driven by non-electrostatic forces, such as the cation–π interaction (Fig. 1).

Although this process effectively encapsulated the pristine SWNTs, the homogeneity and yield of the SWNT/NDI-Bola

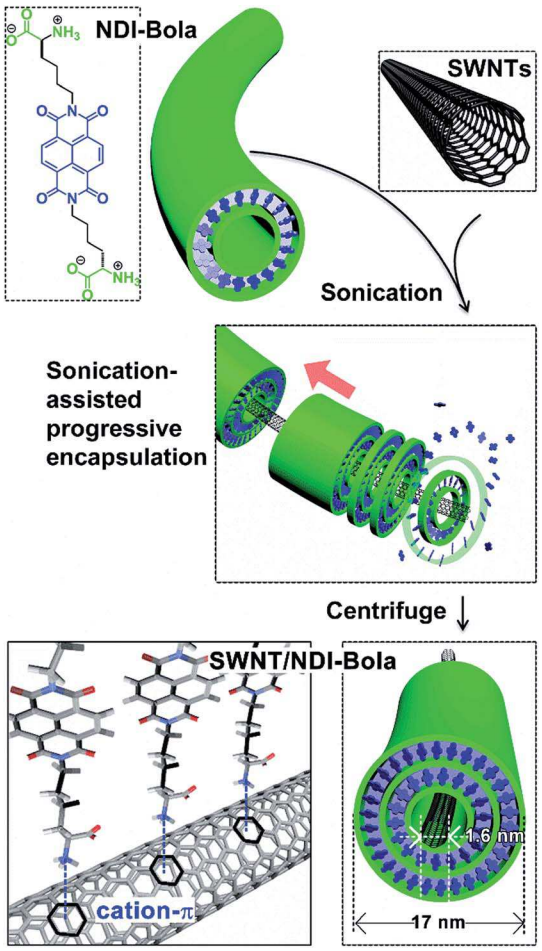

Fig. 1 The assembly of SWNT/NDI-Bola nanotubes. Sonication-induced fragmentation of NDI-Bola nanotubes facilitate threading of the SWNTs through the inner channel of shortened NDI-Bola nanotubes *via* electrostatic and cation–π interactions. The shortened NDI-Bola segments threaded along the SWNT surface gradually merged together *via* self-healing. After incubation, the resulting coaxial SWNT/NDI-Bola assemblies were separated from uncomplexed SWNTs and excess NDI-Bola nanotubes by centrifuging at 5000 rpm.

Open Access Article. Published on 01 August 2019. Downloaded on 10/13/2019 1:23:07 AM.
This article is licensed under a Creative Commons Attribution-NonCommercial 3.0 Unported Licence.

composite was limited by the presence of amorphous carbon impurities, metallic catalyst particles with carbon shells, and remaining bundled/knotted carbon nanotubes (Fig. S1 and S2†). In order to improve the coaxial encapsulation, the pristine SWNTs were polished and de-bundled by an acid treatment (H_2SO_4/HNO_3 3 : 1 at 70 °C)[62,63] prior to mixing with precursor NDI-Bola nanotubes. This debundling process converted the SWNTs into shorter, individual strands (<500 nm) with open ends (Fig. S19†). The preformed NDI-Bola nanotubes exhibited a positive ζ-potential (56.3 ± 4.0 mV; 2 mM, pH 3.46), whereas, the acid-polished SWNTs showed a negative ζ-potential (−48.0 ± 6.1 mV; 2 mM, pH 3.64) (Fig. S4†), due to the presence of carboxylate groups at the nanotube ends. Thus, the encapsulation would also be enhanced by complementary electrostatic interactions between the SWNTs and the NDI-Bola nanotube.

We reasoned that the SWNTs would more efficiently thread through shortened segments of the NDI-Bola nanotubes, as compared with the natively formed, longer nanotubes. Previously, we observed that sonication-induced cavitation was capable of cleaving the NDI-Bola nanotubes (~250–1000 nm), into short nanotube fragments (≤100 nm).[64] These shortened, metastable nanotubes re-assembled into their prior elongated states over time through a self-healing process. Based on this observation, shortened segments would be able to grow and merge together along the SWNT surface to create a continuous, coaxial supramolecular coating. Accordingly, polished SWNTs suspended in water were mixed with preassembled NDI-Bola nanotubes, then the mixture was successively sonicated three times (10% of the maximum amplitude, 100 watts, ultrasonic probe operated at 22.5 kHz) for 10 min. Each round of sonication was followed by a 6 h incubation period at 25 °C to induce self-healing/elongation of the nanotube fragments. After a final 12 h incubation, the SWNT/NDI-Bola composite formed a self-supporting hydrogel (Fig. S6†), which was diluted and pelleted by centrifugation (5000 rpm), yielding the SWNT/NDI-Bola composite containing ~3 wt% of SWNTs. The resulting pellet and supernatants were analyzed by UV, fluorescence and Raman spectroscopy, and imaged by TEM (Fig. 2–5).

Evidence for the co-assembly of NDI-Bola nanotubes and the SWNTs in the centrifuged pellets of the composite was apparent in the absorption and fluorescence spectra (Fig. 2 and S6†). UV-Vis spectra of the aqueous dispersion of SWNT/NDI-Bola pellets exhibited red-shifts of 9 and 15 nm of band I (342, 359, 380 nm) and band II (234 nm) of the NDI chromophore, respectively, compared with monomeric NDI-Bola in TFE. The resemblance of these red-shift peaks to that of the parent NDI-Bola nanotubes in water were indicative of a similar J-type packing present in the composite.[56] The broad absorption band of SWNTs in the composite and the intensified scattering due to the formation of a microgel increased the overall absorption of SWNT/NDI-Bola composite. The supernatant displayed a slightly blue-shifted, low intensity peak attributed to a low concentration of NDI-Bola, in both nanotube and monomeric form (Fig. S6a†). It is important to note that, in contrast to the SWNT/NDI-Bola composite, neither the NDI-Bola nanotubes nor monomer form a pellet upon centrifugation at 5000 rpm. The emission spectra of NDI-Bola nanotubes in water was characterized by

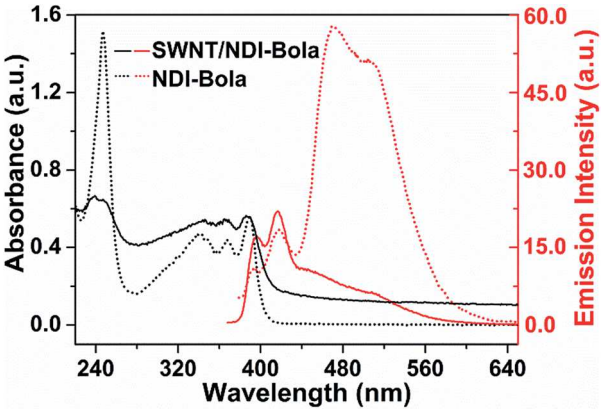

Fig. 2 Absorption (black) and emission (red) spectra of SWNT/NDI-Bola (solid) and NDI-Bola (dashed) in water. The concentrations of NDI-Bola in all samples were 250 μM for UV-Vis and 1 mM for emission studies. All emission experiments were performed using 350 nm excitation.

a relatively strong, low energy emission band at 450–525 nm. In contrast, encapsulation of the SWNTs with NDI-Bola substantially quenched the low energy emission band of NDI-Bola nanotubes, with only the weak emission bands of the molecularly dissolved NDI-Bola at 388 and 410 nm remaining (Fig. S6b†). The quenching of the NDI-Bola emission indicated

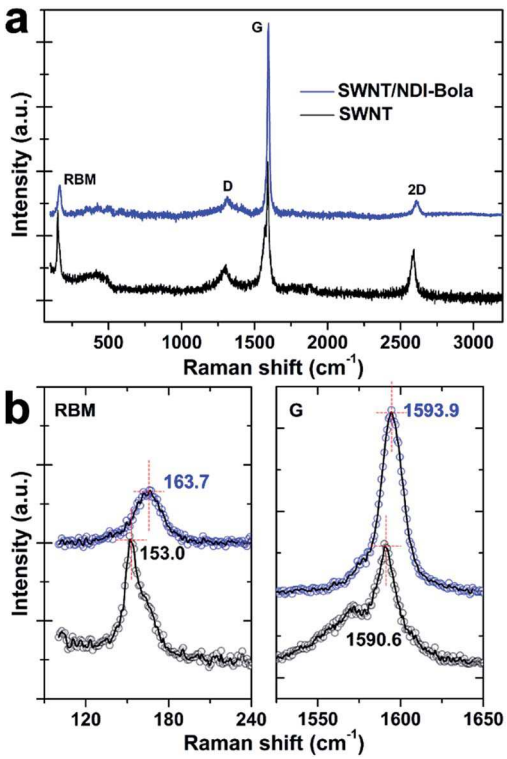

Fig. 3 (a) Raman spectra of aqueous suspensions of de-bundled SWNTs (black) and SWNT/NDI-Bola composites (blue) excited at 785.0 nm (1.58 eV). (b) The radial breathing mode (RBM) and tangential G-band of the de-bundled SWNTs (black) and SWNT/NDI-Bola composites (blue). The spectra values shown represent the average of at least ten measurements for each sample.

This journal is © The Royal Society of Chemistry 2019

Open Access Article. Published on 01 August 2019. Downloaded on 10/13/2019 1:23:07 AM.
This article is licensed under a Creative Commons Attribution-NonCommercial 3.0 Unported Licence.

a close spatial relationship between the NDI-Bola nanotube and the SWNTs, which permitted photoinduced electron or energy-transfer.

Raman spectra provided more insightful information about the spatial alignment within SWNT/NDI-Bola composite (Fig. 3). The encapsulation of the SWNTs by NDI-Bola affected the vibration frequencies of both the radial (RBM) and tangential (G-band) movement of carbon atoms. After mixing with the NDI-Bola nanotubes, the RBM and G-band of SWNTs shifted from 153.0 ± 1.2 and 1590.6 ± 0.8 cm^{-1} to 163.7 ± 1.3 and 1593.9 ± 0.9 cm^{-1} (Fig. 3b and S22†), respectively, indicating an increase in the elastic constant of vibrating carbon atoms in SWNTs due to the formation of an NDI-Bola coating around the SWNTs.[65,66] Also, there was little broadening of the RBM and G-bands in the composite, indicating the homogeneity of the NDI-Bola layer around the carbon nanotubes. The intensity ratio of D-band to G-band (I_D/I_G) increased from 0.24 for SWNTs to 0.35 for SWNT/NDI-Bola. The enhancement of the D-band can be attributed to the field disturbance and physical strain on the graphite skeleton of SWNTs encapsulated by NDI-Bola, or slight damage to the carbon lattice caused by sonication treatments during the preparation of SWNT/NDI-Bola composites.[65,67]

TEM imaging of the SWNT/NDI-Bola mixture after sonication-induced fragmentation of the NDI-Bola nanotubes, as a function of the incubation time, revealed a progressive elongation of NDI-Bola wrapping layers around the SWNTs (Fig. 4). For example, immediately after applying the first sonication treatment (10% amplitude) to the mixture of SWNTs and preformed NDI-Bola nanotubes, SWNTs partly covered by NDI-Bola segments were observed throughout the sample. However, a considerable amount of bare SWNTs randomly laid across the surface of shortened NDI-Bola nanotubes were also present (Fig. 4a). To enhance the ability of the SWNTs to thread the nanotubes, additional sonication treatments were applied to the sample to generate more shortened NDI-Bola nanotubes. Accordingly, a second identical sonication treatment was applied, and the resulting mixture was imaged after incubating for 0, 3 and 6 h (Fig. 4b). A progression from SWNT encapsulated by short NDI-Bola to longer composite nanotubes from 0–6 h could be observed in the TEM images. Moreover, the images qualitatively revealed more co-axial SWNT/NDI-Bola structures and the short NDI-Bola segments sliding along SWNTs were observed to gradually merge into a continuous wrapping layer around the SWNTs. After applying the third sonication, the resulting mixture was incubated for 12 h to complete the assembly of co-axial SWNT/NDI-Bola composite (Fig. 4c). Upon the completion of assembly, the surface of SWNTs was fully covered by NDI-Bola to form co-axial SWNT/NDI-Bola assemblies with diameters of ~17 nm. Additional NDI-Bola nanotubes (12 nm in diameter) and a few isolated SWNTs were also observed in the mixture (Fig. 4c). The resulting mixture was diluted with water and centrifuged (5000 rpm) to collect the

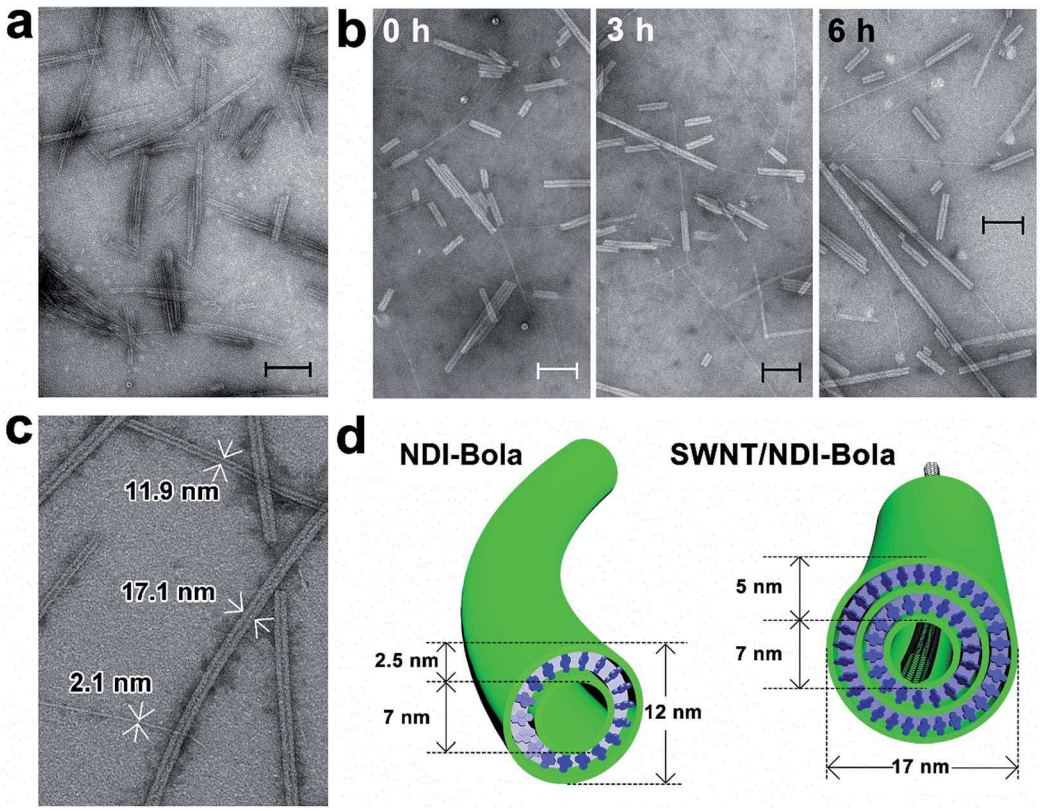

Fig. 4 Progressive morphological changes of the SWNT/NDI-Bola composite: TEM images of the mixture of SWNTs and preformed NDI-Bola nanotubes (a) shortly after the 1st sonication, (b) after the 2nd sonication and incubated for 0, 3 and 6 h, and (c) after the 3rd sonication and incubated for 12 h. Scale bars: 100 nm. (d) Structures of NDI-Bola nanotubes and co-axial SWNT/NDI-Bola composite.

Open Access Article. Published on 01 August 2019. Downloaded on 10/13/2019 1:23:07 AM
This article is licensed under a Creative Commons Attribution-NonCommercial 3.0 Unported Licence

SWNT/NDI-Bola composite in the pellet. This resulted in the selective pelleting of the composite nanotubes, whereas excess NDI-Bola and a few isolated SWNTs remained in the supernatant (Fig. 5a). A semiquantitative comparison of the UV spectra of obtained pellets after each stepwise sonication–incubation cycle indicated that three cycles were sufficient to complete the self-assembly of SWNT/NDI-Bola (Fig. S8†). During the first two sonication–incubation cycles, the amount of SWNT/NDI-Bola composite collected in pellets increased significantly after each sonication/incubation cycle, and the yield of SWNT/NDI-Bola remained stable after the third sonication.

TEM imaging of the SWNT/NDI-Bola pellet revealed uniform nanotubes showing a 5 nm increase in diameter from 12 ± 1 nm, for the elongated NDI-Bola nanotube as the precursor, to 17 ± 1 nm for the coaxial SWNT/NDI-Bola composite (Fig. 5a). The increase in diameter emerged from the thicker walls of SWNT/NDI-Bola, which doubled from 2.5 ± 0.5 (NDI-Bola nanotubes) to 5.0 ± 0.5 nm. The two-fold increase in wall thickness suggests the formation of a bilayer NDI-Bola coating around SWNTs in the SWNT/NDI-Bola composite, in contrast to the monolayer wall structure of the parent NDI-Bola nanotubes. The excess NDI-Bola nanotubes left in the supernatant (Fig. 5b) exhibited the characteristic appearance of nanotubes as two white, parallel lines separated by a dark center, due to their hollow tubular interior (~7 nm). The high-resolution TEM image of the negatively stained SWNT/NDI-Bola composite (Fig. 5a, inset) clearly showed the presence of a single SWNT within the interior of SWNT/NDI-Bola as a thin white line located in the hollow channel of coaxial SWNT/NDI-Bola assemblies. In contrast to the change in wall thickness, the internal dimensions remained constant at ~7 nm. The XRD pattern of the SWNT/NDI-Bola composite (Fig. 6a) showed a sharp reflection with a *d* spacing of 2.10 nm, similar to the low-angle peak of parent NDI-Bola nanotubes (d = 2.17 nm) (Fig. S10b†). These reflections correlated with the length of an extended NDI-Bola molecule (2.3 nm) and the thickness of a monolayer lipid membrane (MLM) of the parent NDI-Bola nanotube, which was comprised of obliquely packed NDI-Bola (2.5 ± 0.5 nm).[56] The peaks at 3.60, 4.32 and 5.41 Å in the XRD pattern of SWNT/NDI-Bola were similar to the diffraction peaks exhibited by the parent NDI-Bola (3.62, 4.35 and 5.52 Å). These reflections correspond to the mean interplanar distance between adjacent planes of the NDI core, and the centroid–centroid distance between nearest-neighbor NDI chromophores (Fig. 6b).[68,69] Moreover, the circular dichroism (CD) spectra of the SWNT/NDI-Bola composite and the parent NDI-Bola nanotubes were nearly identical (Fig. S11†),[56] demonstrating that the NDI-Bola molecules adopted a similar long-range order.

The dimensions of the SWNT/NDI-Bola composite extracted from the TEM images (Fig. 5a) lead to a model with a ~2.5 nm

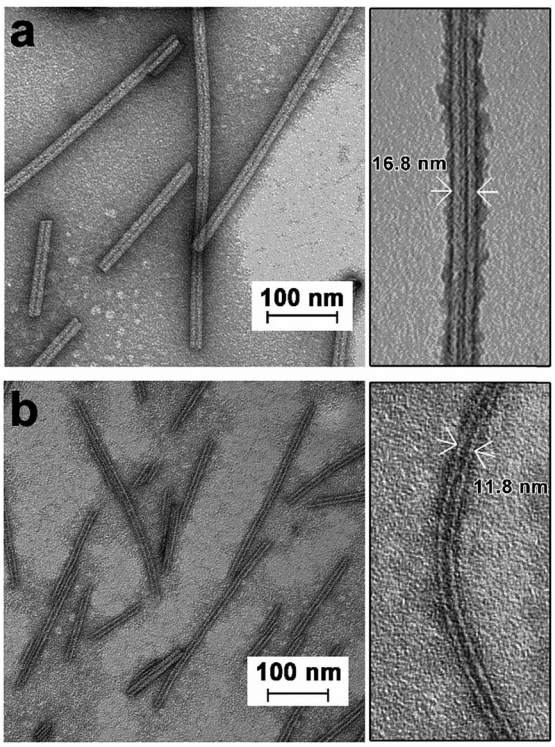

Fig. 5 TEM images of (a) SWNT/NDI-Bola composite collected from pellets after centrifuge (5000 rpm, 10 min) and (b) excess NDI-Bola nanotubes left in the corresponding supernatant. TEM insets: high-resolution images of co-axial SWNT/NDI-Bola and individual NDI-Bola nanotubes. 2% (w/w) uranyl acetate as the negative stain.

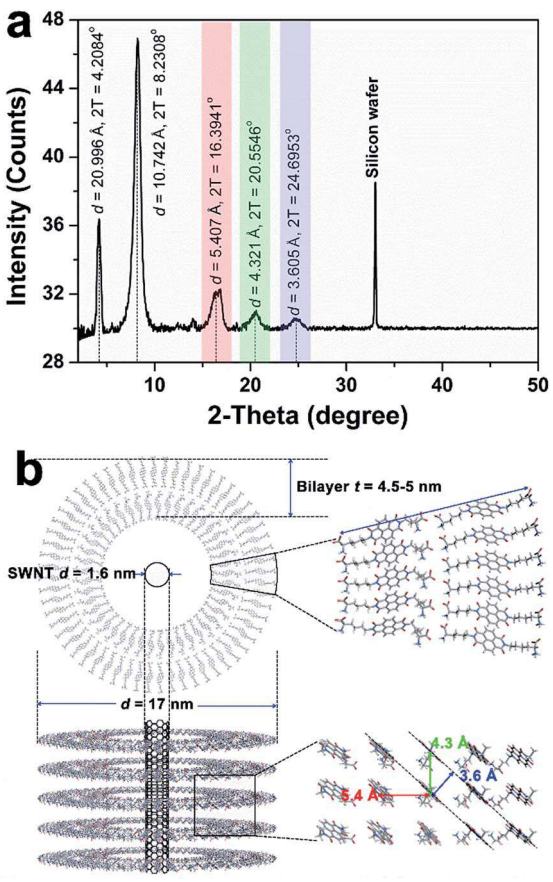

Fig. 6 (a) Representative XRD pattern of the SWNT/NDI-Bola composite cast on monocrystalline silicon wafer. (b) Schematic representations of the co-axial assembly of SWNT/NDI-Bola composite. *d* and *t* indicate nanotube diameters and wall thicknesses.

This journal is © The Royal Society of Chemistry 2019

Open Access Article. Published on 01 August 2019. Downloaded on 10/13/2019 1:23:07 AM.
This article is licensed under a Creative Commons Attribution-NonCommercial 3.0 Unported Licence.

separation between the NDI-Bola inner walls and the surface of the SWNTs, as positioned at the center of the nanotube pore (Fig. 4d and 6b). This separation would not allow for uniform contact between the SWNT surface and the inner walls of NDI-Bola nanotubes. The formation of an initial NDI-Bola layer *via* NDI-SWNT stacking, rather than cation–π interactions could potentially bridge the gap, thereby alleviating the discrepancy. This well-known NDI–SWNT assembly mode[70–72] would also create a hydrophilic SWNT surface that would be more compatible with the polar NDI-Bola nanotube interior. However, inspection of the TEM images of the composite revealed SWNT diameters of 2.1–2.3 nm, similar to the starting dimensions of the debundled SWNTs (Fig. 4c, S19 and S20†). This alternative NDI packing arrangement would also be expected to produce a significant change in the CD spectra of NDI-Bola upon encapsulation of SWNTs, which was not observed (Fig. S11†). As shown in the TEM images of the composite, the SWNT was located much closer to one side of the internal pore of the composite, indicating the presence of an unfilled, spatial gap with the adjacent wall (Fig. 5a and S20a†). Colloidal particles such as the SWNT and NDI-Bola nanotubes carry electrostatic surface charge that is distributed over several nanometers in diffuse electrical double layers (EDL).[73] The overlap of these electric fields on oppositely charged particles strongly affects the stability of colloidal mixtures.[73] To evaluate the EDL interaction in the SWNT/NDI-Bola composite, the ζ-potentials of dispersions of NDI-Bola, de-bundled SWNTs, and the SWNT/NDI-Bola composite were measured (Fig. S4 and S12†). A sample of the SWNT/NDI-Bola hydrogel (10 mM), diluted to 2 mM, exhibited a ζ-potential of 24.3 ± 2.6 mV at pH 3.5, while the parent NDI-Bola nanotubes and debundled SWNTs maintained ζ-potentials of 56.3 ± 4.0 mV (pH 3.46) and −48.0 ± 6.1 mV (pH 3.64) (Fig. S4†), respectively. Although the change in ζ-potential was small for the encapsulation of pristine SWNTs by the NDI-Bola, the large negative Δζ observed for the debundled SWNTs indicated a strong EDL interaction over the spatial separation of the SWNT and NDI-Bola surfaces.

The change to a bilayer wall structure likely emerged as a response to the reduction in ζ-potential during assembly of the composite. Colloidal dispersions of self-assembled particles are thermodynamically unstable relative to larger particles with lower interfacial area per mass.[74,75] The stability of colloidal dispersions observed in many systems is a kinetic phenomenon reflecting the interplay between repulsive EDL and attractive van der Waals forces between the particles, as described by DLVO theory.[76] Thus, the monolayer to bilayer transition in the SWNT/NDI-Bola walls ensued from a change in the balance of these forces. The high ζ-potential of the NDI-Bola nanotubes stabilized the dispersion, relative to larger aggregates, by repulsive EDL interactions. The lower surface charge of the composite structure permitted two NDI-Bola monolayers to merge, thereby forming a larger nanotube with lower total surface area.

The ability of the composite to adapt to the reduced surface charge is a dynamic equilibrium process, requiring the presence of small amounts of free NDI-Bola monomer to proceed. In fact, the supernatant of ultracentrifuged samples of preassembled nanotubes were shown to contain monomeric NDI-Bola (Fig. S13†). To qualitatively explore the role of monomer in the formation of the composite, free monomer was removed *via* ultracentrifuge (80 000 rpm) and the resultant pellet was redispersed, mixed with the SWNTs and subjected to the sonication/incubation sequence. Centrifugation (5000 rpm) of the mixture did not produce a pellet and TEM imaging of the sample showed only the formation of the parent NDI-Bola nanotubes with little evidence of composite nanostructures (Fig. S17†). Although it is not possible to unambiguously remove monomer from the nanotubes, the co-assembly process was significantly less efficient in this experiment.

The outstanding mechanical properties of SWNTs, such as the exceptionally high Young's modulus, make them promising as reinforcements in polymer composites.[77] The threading of SWNTs within the composite would be expected to increase the modulus, compared with the parent NDI-Bola nanotubes. Young's modulus of the parent NDI-Bola and the SWNT/NDI-Bola were measured by PeakForce quantitative nanomechanical mapping (QNM), which confirmed a larger modulus for the SWNT/NDI-Bola composite (Fig. 7). QNM, an atomic force microscopy (AFM) technique based on the Derjaguin–Muller–Toporov (DMT) model, enables the measurement of Young's modulus with high spatial resolution, by probing the tip–sample interaction at the nanoscale.[78] AFM imaging indicated shorter lengths of SWNT/NDI-Bola composite, compared with the parent nanotubes (Fig. 7a and d), as a consequence of the shorter length distribution of polished SWNTs (200–500 nm). The modulus distributions of NDI-Bola (Fig. 7c) and SWNT/NDI-Bola (Fig. 7f) modulus were calculated based on measurements of ≥500 individual filaments. After treatment with SWNTs, the peak of Young's modulus distribution increased from 1.7 GPa for the precursor NDI-Bola nanotubes to 2.8 GPa for the SWNT/NDI-Bola composite. The narrower DMT modulus distribution of the SWNT/NDI-Bola (FWHM 1.0 GPa), compared with that of the NDI-Bola nanotubes (FWHM 1.2 GPa), reflected the higher homogeneity of the SWNT/NDI-Bola composite.

The assembly of nanostructured composites having multiple, sorted domains are particularly important for optoelectronic materials. Previously, we reported an electrostatic layer-by-layer process to assemble coaxial, nanotube–polymer composites, capable of undergoing photoinduced charge separation.[14] To explore the potential to create coaxial nanostructures integrated with a SWNT using this strategy, water-soluble poly(*p*-phenyleneethynylene) (PPE-SO_3Na, $M_W = 5.76 \times 10^4$, PDI – 1.11) was added to the SWNT/NDI-Bola composite to serve as the outer layer of the ternary composite. The SWNT/NDI-Bola composite exhibited a positive ζ-potential below the isoelectric pH (pI 3.8, Fig. S12†). A pelleted sample of SWNT/NDI-Bola in water (2 mM) displayed a pH ∼ 3.5, resulting in a slightly positive ζ-potential. A corresponding complementary electrostatic attraction with negatively charged PPE-SO_3Na was expected to drive formation of the ternary composite. Accordingly, a 2.5 nm increase in the diameter of SWNT/NDI-Bola/PPE-SO_3Na, compared with the SWNT/NDI-Bola precursor (Fig. 8c), was observed upon addition of PPE-SO_3Na to the composite

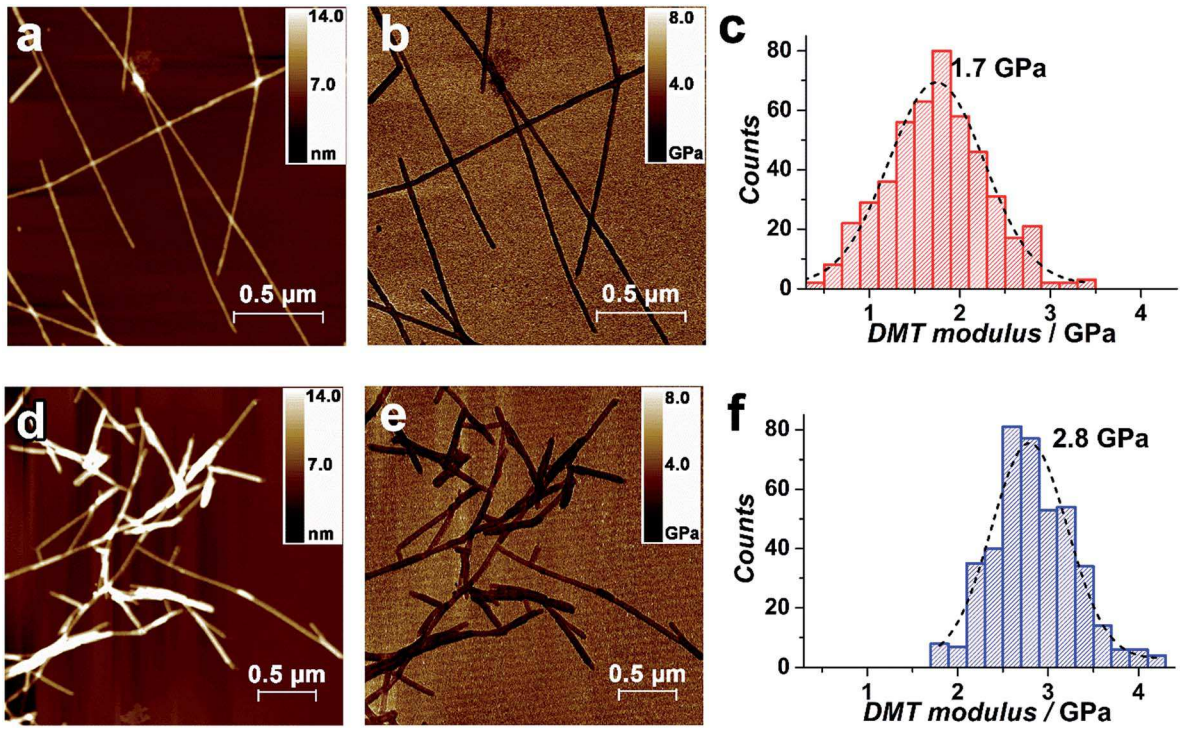

Fig. 7 Height profile and Derjaguin–Muller–Toporov (DMT) modulus AFM images of (a and b) NDI-Bola and (d and e) SWNT/NDI-Bola deposited on freshly cleaved mica. (c and f) Distributions of DMT modulus of (c) NDI-Bola and (f) SWNT/NDI-Bola fit single Gaussian peaks at 1.7 GPa with 1.2 GPa full width at half-maximum (FWHM) and at 2.8 GPa with 1.0 GPa FWHM, respectively.

(10 : 1 SWNT/NDI-Bola: PPE-SO_3Na). The resulting ternary composite, pelleted by centrifugation, displayed a new UV-Vis absorption at 450 nm (Fig. 8a) arising from the presence of the PPE-SO_3Na coating. To determine the amount of polymer to reach surface saturation, the feeding ratio of NDI-Bola, in the SWNT/NDI-Bola composite, to the PPE-SO_3Na polymer was varied (composite : PPE-SO_3Na; 10 : 0.5, 10 : 1, and 10 : 2). These experiments were performed by preparing the SWNT/NDI-Bola composite, as described above, and pelleting by centrifugation. The pellet was diluted and treated with varying amounts of PPE-SO_3Na, and pelleted. Considering the loss of NDI-Bola in the supernatant during preparation of SWNT/NDI-Bola, the final composite : PPE-SO_3Na ratios were adjusted to 10 : 0.6, 10 : 1.2 and 10 : 2.4. Inspection of the UV-Vis spectra of the pellets indicated a maximal polymer coating level was achieved at a 10 : 1 feeding ratio (Fig. S16a†).

The deposition of the polymer on the surface of the SWNT/NDI-Bola composite was analogous to the assembly of polyelectrolyte multilayers, which are formed by the alternating deposition of oppositely charged polymers.[79] Similarly, polymer binding to the surface of the composite was driven primarily by electrostatic interactions along with the associated entropic

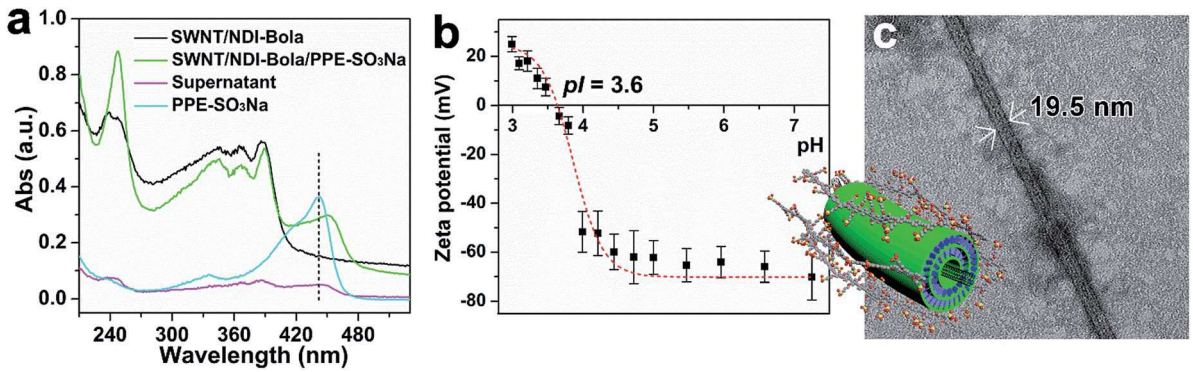

Fig. 8 (a) UV-Vis spectra of SWNT/NDI-Bola (black), SWNT/NDI-Bola/PPE-SO_3Na (10 : 1 NDI-Bola/PPE-SO_3Na, green) and corresponding supernatant (magenta) after centrifuge at 5000 rpm for 15 min. The concentration of NDI-Bola in all samples was *ca.* 250 μM. As a comparison, PPE-SO_3Na (25 μM in water) is shown in cyan. (b) ζ-Potential titration curve of SWNT/NDI-Bola/PPE-SO_3Na (10 : 1, 2 mM with respect to NDI-Bola) composite in water at 25 °C. The dashed curve is given for eye guidance. (c) TEM image of SWNT/NDI-Bola/PPE-SO_3Na (10 : 1). 2% (w/w) uranyl acetate as the negative stain.

This journal is © The Royal Society of Chemistry 2019

Open Access Article. Published on 01 August 2019. Downloaded on 10/13/2019 1:23:07 AM.
This article is licensed under a Creative Commons Attribution-NonCommercial 3.0 Unported Licence.

gain associated with counterion release. The ζ-potential of the SWNT/NDI-Bola/PPE-SO_3Na composite exhibited a pH dependent profile similar to the SWNT/NDI-Bola precursor (Fig. 8b). However, due to the presence of the PPE-SO_3Na, the ternary composite maintained a slightly lower isoelectric point (pI 3.6). At pH values above the pI, ζ-potential values were 20–30 mV lower than for the SWNT/NDI-Bola precursor. The efficacy of polymer binding at pH values above the pI suggested that non-electrostatic adsorptions, such as polarization-induced attraction,[80–82] might also contribute to the polymer binding process. In order to investigate the stability of the ternary composite, fluorescence emission of the PPE-SO_3Na polymer at 525 nm was recorded as a function of pH (Fig. S16b and c†). The strong emission at 525 nm was almost completely quenched due to electron/energy transfer within the confines of the ternary structure over a pH range of 3–7. At pH 10, the emission of PPE-SO_3Na was restored instantly, indicating the dissociation of PPE-SO_3Na from the composite. It is noteworthy that the NDI-Bola nanotubes (pI 6.7) also bind PPE-SO_3Na (10 : 1, n/n) at pH 3.6 (Fig. S23†). However, the pH-dependence of fluorescence emission (pH 4–12, Fig. S23c†) revealed that the NDI-Bola/PPE-SO_3Na interaction was stronger than that of SWNT/NDI-Bola/PPE-SO_3Na. The higher stability was manifested by a partial increase in emission intensity (525 nm) at pH 11 (Fig. S23c†), compared to the large increase in emission at pH 10 for the SWNT/NDI-Bola/PPE-SO_3Na composite (Fig. S16c†). The difference in binding affinity emanated from the higher pI of the NDI-Bola nanotubes (Fig. S23d†), which allowed for a stronger electrostatic interaction over a broader pH range.

Conclusions

In this work, we have described the co-assembly of a well-defined, multicomponent nanostructure comprised of a SWNT encapsulated by a self-assembled NDI nanotube, and subsequently wrapped by a PPE-SO_3Na polymer layer. We have shown that the polar interior of the self-assembled nanotubes accommodates the hydrophobic surface of the SWNT through a combination of cation–π and electrostatic interactions. The threading process was facilitated by sonication-induced fragmentation of the NDI-Bola nanotube, followed by elongation and merging of the nanotube segments into a homogeneous array of fully coated SWNTs. Centrifugation of the mixture separated the composite nanostructure from the individual components, resulting in a pure sample of the SWNT/NDI-Bola composite containing ~3 wt% of carbon nanotubes. The ζ-potential of the SWNT/NDI-Bola was adjusted by pH to electrostatically interact with complementary polyelectrolyte polymers wrapped around the outer surface. This work sets the stage for the design and assembly of hierarchically ordered, multicomponent nanostructures for use in a wide range of potential applications ranging from optoelectronics to biomedicine.

Conflicts of interest

There are no conflicts to declare.

Acknowledgements

We acknowledge the technical assistance and usage of the AFM facility at the Ohio State Surface Analysis Lab. This work was supported by the National Science Foundation (CHE-1708390 and CHE-1708388).

Notes and references

1 M. R. Wasielewski, *Chem. Rev.*, 1992, **92**, 435–461.
2 D. Gust, T. A. Moore and A. L. Moore, *Acc. Chem. Res.*, 2009, **42**, 1890–1898.
3 X. Liu, S. Inagaki and J. Gong, *Angew. Chem.*, 2016, **55**, 14924–14950.
4 C. J. Wilson, A. S. Bommarius, J. A. Champion, Y. O. Chernoff, D. G. Lynn, A. K. Paravastu, C. Liang, M. C. Hsieh and J. M. Heemstra, *Chem. Rev.*, 2018, **118**, 11519–11574.
5 Y. Sun, J. A. Kaplan, A. Shieh, H.-L. Sun, C. M. Croce, M. W. Grinstaff and J. R. Parquette, *Chem. Commun.*, 2016, **52**, 5254–5257.
6 H. Cui and B. Xu, *Chem. Soc. Rev.*, 2017, **46**, 6430–6432.
7 K. S. Lee and J. R. Parquette, *Chem. Commun.*, 2015, **51**, 15653–15656.
8 S. Satagopan, Y. Sun, J. R. Parquette and F. R. Tabita, *Biotechnol. Biofuels*, 2017, **10**, 175.
9 C. Q. Zhang, X. D. Xue, Q. Luo, Y. W. Li, K. N. Yang, X. X. Zhuang, Y. G. Jiang, J. C. Zhang, J. Q. Liu, G. Z. Zou and X. J. Liang, *ACS Nano*, 2014, **8**, 11715–11723.
10 Z. Lengyel, C. M. Rufo, Y. S. Moroz, O. V. Makhlynets and I. V. Korendovych, *ACS Catal.*, 2018, **8**, 59–62.
11 S. Bhowmick, L. Zhang, G. Ouyang and M. Liu, *ACS Omega*, 2018, **3**, 8329–8336.
12 S. Tu, S. H. Kim, J. Joseph, D. A. Modarelli and J. R. Parquette, *J. Am. Chem. Soc.*, 2011, **133**, 19125–19130.
13 A. M. Sanders, T. J. Magnanelli, A. E. Bragg and J. D. Tovar, *J. Am. Chem. Soc.*, 2016, **138**, 3362–3370.
14 M. Y. Ji, M. B. Dawadi, A. R. LaSalla, Y. Sun, D. A. Modarelli and J. R. Parquette, *Langmuir*, 2017, **33**, 9129–9136.
15 R. N. Perham, *Philos. Trans. R. Soc. London, Ser. B*, 1975, **272**, 123–136.
16 Y. Guo, L. Xu, H. Liu, Y. Li, C. M. Che and Y. Li, *Adv. Mater.*, 2015, **27**, 985–1013.
17 A. T. Haedler, S. C. Meskers, R. H. Zha, M. Kivala, H. W. Schmidt and E. W. Meijer, *J. Am. Chem. Soc.*, 2016, **138**, 10539–10545.
18 S. Ogi, T. Fukui, M. L. Jue, M. Takeuchi and K. Sugiyasu, *Angew. Chem.*, 2014, **53**, 14363–14367.
19 A. Lohr and F. Wurthner, *Isr. J. Chem.*, 2011, **51**, 1052–1066.
20 D. Gorl, X. Zhang, V. Stepanenko and F. Wurthner, *Nat. Commun.*, 2015, **6**, 7009.
21 S. Y. Tu, S. H. Kim, J. Joseph, D. A. Modarelli and J. R. Parquette, *J. Am. Chem. Soc.*, 2011, **133**, 19125–19130.
22 R. Charvet, Y. Yamamoto, T. Sasaki, J. Kim, K. Kato, M. Takata, A. Saeki, S. Seki and T. Aida, *J. Am. Chem. Soc.*, 2012, **134**, 2524–2527.

Open Access Article. Published on 01 August 2019. Downloaded on 10/13/2019 1:23:07 AM.
This article is licensed under a Creative Commons Attribution-NonCommercial 3.0 Unported Licence.

23 W. Wang, Y. Zhang, B. Sun, L.-J. Chen, X.-D. Xu, M. Wang, X. Li, Y. Yu, W. Jiang and H.-B. Yang, *Chem. Sci.*, 2014, **5**, 4554–4560.
24 Y. Hirai, T. Terashima, M. Takenaka and M. Sawamoto, *Macromolecules*, 2016, **49**, 5084–5091.
25 L. J. Chen and H. B. Yang, *Acc. Chem. Res.*, 2018, **51**, 2699–2710.
26 D. M. Raymond and B. L. Nilsson, *Chem. Soc. Rev.*, 2018, **47**, 3659–3720.
27 Z. Y. Zhou, X. W. Chen and S. Holdcroft, *J. Am. Chem. Soc.*, 2008, **130**, 11711–11718.
28 P. Peumans, S. Uchida and S. R. Forrest, *Nature*, 2003, **425**, 158–162.
29 A. Kira, T. Umeyama, Y. Matano, K. Yoshida, S. Isoda, J. K. Park, D. Kim and H. Imahori, *J. Am. Chem. Soc.*, 2009, **131**, 3198–3200.
30 A. L. Sisson, N. Sakai, N. Banerji, A. Furstenberg, E. Vauthey and S. Matile, *Angew. Chem.*, 2008, **47**, 3727–3729.
31 F. Würthner, Z. J. Chen, F. J. M. Hoeben, P. Osswald, C. C. You, P. Jonkheijm, J. von Herrikhuyzen, A. P. H. J. Schenning, P. P. A. M. van der Schoot, E. W. Meijer, E. H. A. Beckers, S. C. J. Meskers and R. A. J. Janssen, *J. Am. Chem. Soc.*, 2004, **126**, 10611–10618.
32 P. Jonkheijm, N. Stutzmann, Z. J. Chen, D. M. de Leeuw, E. W. Meijer, A. P. H. J. Schenning and F. Würthner, *J. Am. Chem. Soc.*, 2006, **128**, 9535–9540.
33 W. S. Li, Y. Yamamoto, T. Fukushima, A. Saeki, S. Seki, S. Tagawa, H. Masunaga, S. Sasaki, M. Takata and T. Aida, *J. Am. Chem. Soc.*, 2008, **130**, 8886–8887.
34 R. S. K. Kishore, O. Kel, N. Banerji, D. Emery, G. Bollot, J. Mareda, A. Gomez-Casado, P. Jonkheijm, J. Huskens, P. Maroni, M. Borkovec, E. Vauthey, N. Sakai and S. Matile, *J. Am. Chem. Soc.*, 2009, **131**, 11106–11116.
35 A. A. Gorodetsky, C.-Y. Chiu, T. Schiros, M. Palma, M. Cox, Z. Jia, W. Sattler, I. Kymissis, M. Steigerwald and C. Nuckolls, *Angew. Chem.*, 2010, **49**, 7909–7912.
36 Y. Hizume, K. Tashiro, R. Charvet, Y. Yamamoto, A. Saeki, S. Seki and T. Aida, *J. Am. Chem. Soc.*, 2010, **132**, 6628–6629.
37 Y. Che, H. Huang, M. Xu, C. Zhang, B. R. Bunes, X. Yang and L. Zang, *J. Am. Chem. Soc.*, 2011, **133**, 1087–1091.
38 A. J. Clancy, M. K. Bayazit, S. A. Hodge, N. T. Skipper, C. A. Howard and M. S. P. Shaffer, *Chem. Rev.*, 2018, **118**, 7363–7408.
39 S. K. Samanta, M. Fritsch, U. Scherf, W. Gomulya, S. Z. Bisri and M. A. Loi, *Acc. Chem. Res.*, 2014, **47**, 2446–2456.
40 I. F. Silva, W. D. do Pim, I. F. Teixeira, W. P. Barros, A. P. C. Teixeira, G. M. do Nascimento, C. L. Pereira and H. O. Stumpf, *J. Phys. Chem. C*, 2016, **120**, 1245–1251.
41 A. Nakamura, T. Koyama, Y. Miyata and H. Shinohara, *J. Phys. Chem. C*, 2016, **120**, 4647–4652.
42 D. R. Barbero and S. D. Stranks, *Adv. Mater.*, 2016, **28**, 9668–9685.
43 J. Chen, B. Liu, X. Gao and D. Xu, *RSC Adv.*, 2018, **8**, 28048–28085.
44 S. D. Stranks, C.-K. Yong, J. A. Alexander-Webber, C. Weisspfennig, M. B. Johnston, L. M. Herz and R. J. Nicholas, *ACS Nano*, 2012, **6**, 6058–6066.
45 S. D. Stranks, S. N. Habisreutinger, B. Dirks and R. J. Nicholas, *Adv. Mater.*, 2013, **25**, 4365–4371.
46 S. D. Stranks, A. M. Baker, J. A. Alexander-Webber, B. Dirks and R. J. Nicholas, *Small*, 2013, **9**, 2245–2249.
47 M. S. Arnold, M. O. Guler, M. C. Hersam and S. I. Stupp, *Langmuir*, 2005, **21**, 4705–4709.
48 F. A. Mann, J. Horlebein, N. F. Meyer, D. Meyer, F. Thomas and S. Kruss, *Chem.–Eur. J.*, 2018, **24**, 12241–12245.
49 A. López-Moreno, B. Nieto-Ortega, M. Moffa, A. de Juan, M. M. Bernal, J. P. Fernández-Blázquez, J. J. Vilatela, D. Pisignano and E. M. Pérez, *ACS Nano*, 2016, **10**, 8012–8018.
50 E. M. Pérez, *Chem.–Eur. J.*, 2017, **23**, 12681–12689.
51 A. Ortiz-Acevedo, H. Xie, V. Zorbas, W. M. Sampson, A. B. Dalton, R. H. Baughman, R. K. Draper, I. H. Musselman and G. R. Dieckmann, *J. Am. Chem. Soc.*, 2005, **127**, 9512–9517.
52 C.-c. Chiu, M. C. Maher, G. R. Dieckmann and S. O. Nielsen, *ACS Nano*, 2010, **4**, 2539–2546.
53 K. Miki, K. Saiki, T. Umeyama, J. Baek, T. Noda, H. Imahori, Y. Sato, K. Suenaga and K. Ohe, *Small*, 2018, **14**, e1800720.
54 R. Chamorro, L. de Juan-Fernandez, B. Nieto-Ortega, M. J. Mayoral, S. Casado, L. Ruiz-Gonzalez, E. M. Perez and D. Gonzalez-Rodriguez, *Chem. Sci.*, 2018, **9**, 4176–4184.
55 C. Richard, F. Balavoine, P. Schultz, T. W. Ebbesen and C. Mioskowski, *Science*, 2003, **300**, 775–778.
56 H. Shao, J. Seifert, N. C. Romano, M. Gao, J. J. Helmus, C. P. Jaroniec, D. A. Modarelli and J. R. Parquette, *Angew. Chem.*, 2010, **49**, 7688–7691.
57 T. A. Pham, S. M. G. Mortuza, B. C. Wood, E. Y. Lau, T. Ogitsu, S. F. Buchsbaum, Z. S. Siwy, F. Fornasiero and E. Schwegler, *J. Phys. Chem. C*, 2016, **120**, 7332–7338.
58 T. Zhang, H. Matsuda and H. Zhou, *ChemSusChem*, 2014, **7**, 2845–2852.
59 Y.-T. Kim, S. H. Joo, H. Min, J. Lee, S. M. Moon, M. Byeon, T. E. Hong, M. S. Strano, J.-H. Han, S. K. Kwak and C. Y. Lee, *Chem. Mater.*, 2018, **30**, 5184–5193.
60 A. S. Mahadevi and G. N. Sastry, *Chem. Rev.*, 2013, **113**, 2100–2138.
61 J. C. Ma and D. A. Dougherty, *Chem. Rev.*, 1997, **97**, 1303–1324.
62 J. Liu, A. G. Rinzler, H. Dai, J. H. Hafner, R. K. Bradley, P. J. Boul, A. Lu, T. Iverson, K. Shelimov and C. B. Huffman, *Science*, 1998, **280**, 1253–1256.
63 B. Vigolo, C. Hérold, J.-F. Marêché, J. Ghanbaja, M. Gulas, F. Le Normand, R. Almairac, L. Alvarez and J.-L. Bantignies, *Carbon*, 2010, **48**, 949–963.
64 M. Ji, B. Daniels, A. Shieh, D. A. Modarelli and J. R. Parquette, *Chem. Commun.*, 2017, **53**, 12806–12809.
65 V. A. Sinani, M. K. Gheith, A. A. Yaroslavov, A. A. Rakhnyanskaya, K. Sun, A. A. Mamedov, J. P. Wicksted and N. A. Kotov, *J. Am. Chem. Soc.*, 2005, **127**, 3463–3472.
66 Z. Liu, J. Zhang and B. Gao, *Chem. Commun.*, 2009, 6902–6918.
67 Y. Liu, P. Liang, H. Y. Zhang and D. S. Guo, *Small*, 2006, **2**, 874–878.

This journal is © The Royal Society of Chemistry 2019

Open Access Article. Published on 01 August 2019. Downloaded on 10/13/2019 1:23:07 AM.
This article is licensed under a Creative Commons Attribution-NonCommercial 3.0 Unported Licence.

68 M. Tomasulo, D. M. Naistat, A. J. White, D. J. Williams and F. M. Raymo, *Tetrahedron Lett.*, 2005, **46**, 5695–5698.
69 M. Gao, S. Paul, C. D. Schwieters, Z. Q. You, H. Shao, J. M. Herbert, J. R. Parquette and C. P. Jaroniec, *J. Phys. Chem. C*, 2015, **119**, 13948–13956.
70 S. Leret, Y. Pouillon, S. Casado, C. Navio, A. Rubio and E. M. Perez, *Chem. Sci.*, 2017, **8**, 1927–1935.
71 A. de Juan, A. Lopez-Moreno, J. Calbo, E. Orti and E. M. Perez, *Chem. Sci.*, 2015, **6**, 7008–7014.
72 Z. Hu, G. D. Pantoş, N. Kuganathan, R. L. Arrowsmith, R. M. J. Jacobs, G. Kociok-Köhn, J. O'Byrne, K. Jurkschat, P. Burgos, R. M. Tyrrell, S. W. Botchway, J. K. M. Sanders and S. I. Pascu, *Adv. Funct. Mater.*, 2012, **22**, 503–518.
73 K. Bohinc, V. Kralj-Iglic and A. Iglic, *Electrochim. Acta*, 2001, **46**, 3033–3040.
74 Ç. Ç. Cenker, S. Bucak and U. Olsson, *Soft Matter*, 2011, **7**, 4868–4875.
75 J. N. Israelachvili, in *Intermolecular and surface forces*, Elsevier, USA, 3rd edn, 2011, pp. 528–530.
76 B. V. Derjaguin, N. V. Churaev and V. M. Muller, in *Surface Forces*, Springer, US, Boston, MA, 1987, pp. 293–310.
77 B. Arash, Q. Wang and V. K. Varadan, *Sci. Rep.*, 2014, **4**, 6479.
78 T. Young, M. Monclus, T. Burnett, W. Broughton, S. Ogin and P. Smith, *Meas. Sci. Technol.*, 2011, **22**, 125703.
79 V. R. Klitzing, *Phys. Chem. Chem. Phys.*, 2006, **8**, 5012–5033.
80 J. Blaakmeer, M. C. Stuart and G. Fleer, *J. Colloid Interface Sci.*, 1990, **140**, 314–325.
81 A. V. Dobrynin, R. H. Colby and M. Rubinstein, *J. Polym. Sci., Part B: Polym. Phys.*, 2004, **42**, 3513–3538.
82 Y. Tran, P. Perrin, S. Deroo and F. Lafuma, *Langmuir*, 2006, **22**, 7543–7551.